ACS Synthetic Biology

Subscriber access provided by University of Newcastle, Australia

Letter

Engineering Iron Responses in Mammalian Cells by Signal-Induced Protein Proximity

Guihua Zeng, Huanqiu Li, Yongyi Wei, Weimin Xuan, Roushu Zhang, Larisa Elise Breden, Wei Wang, and Fu-Sen Liang

ACS Synth. Biol., **Just Accepted Manuscript** • DOI: 10.1021/acssynbio.6b00255 • Publication Date (Web): 21 Feb 2017

Engineering Iron Responses in Mammalian Cells by Signal-Induced Protein Proximity

Guihua Zeng,[§,‡] Huanqiu Li,[§,†,‡] Yongyi Wei,[§] Weimin Xuan,[§] Roushu Zhang,[§] Larisa E. Breden,[§] Wei Wang*[,§] and Fu-Sen Liang*[,§]

[§]Department of Chemistry and Chemical Biology, University of New Mexico, Albuquerque, NM87131, USA.

[†]Department of Medicinal Chemistry, College of Pharmaceutical Sciences, Soochow University, Suzhou 215123, PR China.

Supporting Information Placeholder

ABSTRACT: A new synthetic biology engineering strategy integrating chemical reactivity sensing and small molecule induced protein dimerization has been developed to generate artificial Fe^{2+} signaling circuitry to control tailored cellular events in mammalian cells. The dual function probe **ABA-FE18** (Fe^{2+}-sensing and protein dimerization) derived from **ABA** was developed and used to control gene activation, signal transduction and cytoskeletal remodeling in response to Fe^{2+}. This technology was utilized to design signal circuitry incorporating "AND" and "OR" biologic gates that enables mammalian cells to translate different combinations of Fe^{2+} and H_2O_2 signals into pre-defined biological outputs.

KEYWORDS: chemically induced proximity, labile iron, biosensor, biologic gate, abscisic acid, cell signaling

The aim of synthetic biology research is to rewire biological systems in order to understand and control the functions of cellular systems that ultimately lead to novel therapies.[1-6] Cell signaling translates extracellular signals into intracellular processes that carry out cellular functions. Introduction of artificial signaling networks using synthetic biology methods has facilitated the investigation of signaling mechanisms and the identification of essential components in signaling pathways.[7-10] Several synthetic biology methods that are based on chemical controls have been developed to provide precise temporal regulation.[1,11] We recently reported a new strategy to engineer custom signaling pathways in mammalian cells that integrates the chemically induced proximity (CIP) technology[12,13] and reactivity-based signal sensing.[14] The approach enables cells to link H_2O_2 or light with different cellular responses including gene activation, protein translocation and cytoskeleton remodeling.[15,16] The method uses caged CIP inducers (e.g. abscisic acid (**ABA**)[17]) that are inactive until being stimulated by a specific signal (e.g. H_2O_2) that removes the caging group and activates an inducer to promote the heterodimerization of selected PYL/ABI fusion proteins. Induced protein dimerization then triggers pre-designed biological outputs. Our continuing investigations in this are aimed at testing the generality of this strategy for creating new signaling pathways for other important stimuli and exploring the possibility of constructing cross-talking pathways. In the study described below, we have developed a method to engineer artificial Fe^{2+} signaling that responds to elevated Fe^{2+} levels and to build "AND" and "OR" Boolean logic-based signaling circuitries that respond to a combination of H_2O_2 and Fe^{2+} in a pre-defined manner.

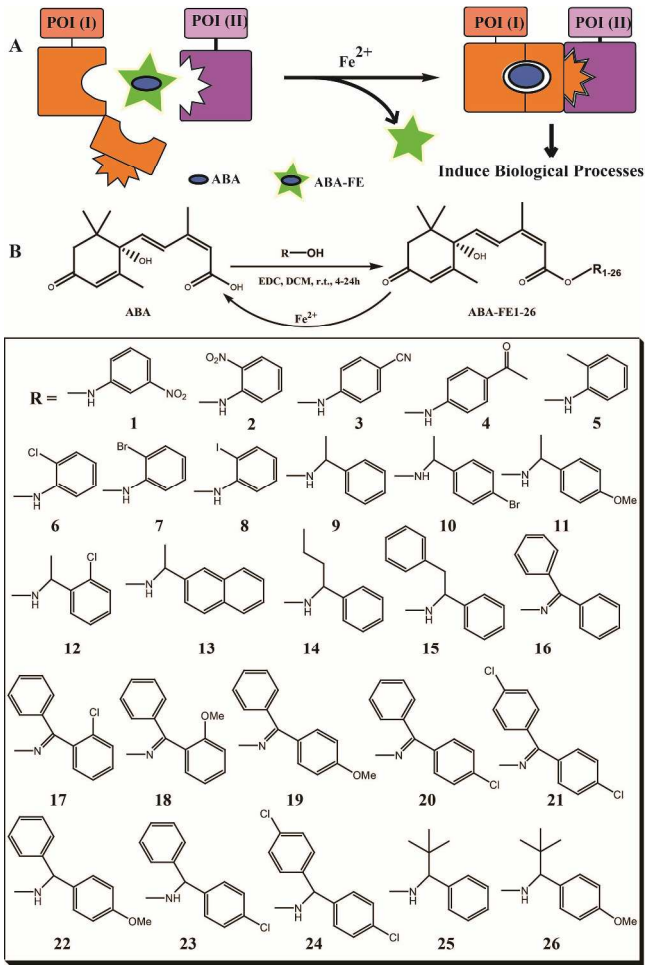

Figure 1. (A) Fe^{2+}-induced protein proximity to control biological processes. (B) Synthesis and the structures of **ABA-FEs**.

Iron is the most abundant transition metal in humans and its redox chemistry interconverting Fe^{2+} and Fe^{3+} plays numerous biological roles.[18] Although most iron ions exist in complexes with proteins, free Fe^{2+} is present in cellular environments where

it is believed to participate in critical physiological functions.[19] An increased level of Fe^{2+} has been observed in brains of patients with neurodegenerative diseases (e.g. Alzheimer's disease (AD) and Parkinson's diseases (PD)).[20] It is proposed that the combination of elevated levels of Fe^{2+} and H_2O_2 (under oxidative stress) leads to the production of free radicals which promote neuron death in AD and PD.[21-23] The availability of an engineered system that enables cells to detect elevated levels of H_2O_2 and Fe^{2+} in local environments and respond with specific therapeutic outputs would contribute to the development of novel therapies for AD and PD.

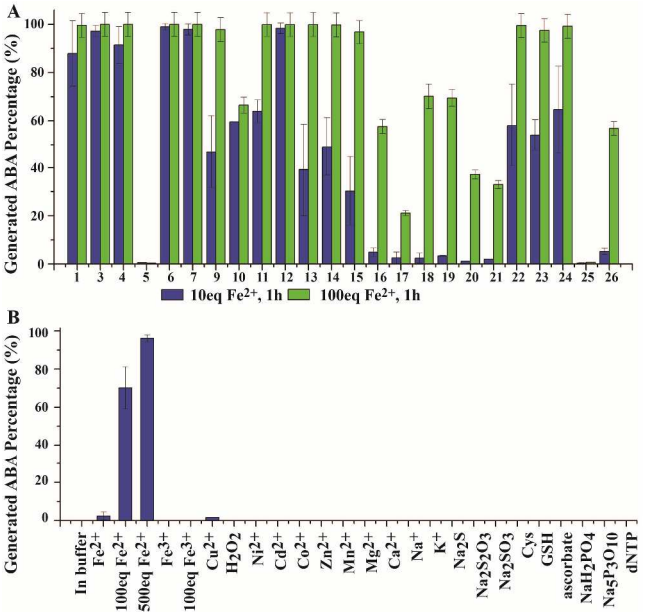

Figure 2. (A) 10 μM **ABA-FEs** were treated with 10 eq and 100 eq Fe^{2+} for 1h respectively and then quantified using HPLC analysis. (B) **ABA-FE18** was treated with indicated ions and molecules (10 eq for all unlabeled items) for 1 h and then quantified using HPLC analysis. Error bars are SD (N = 3).

Several fluorescent probes have been developed to assess the level of Fe^{2+} in living cells.[24-28] Included in this group is the new reactivity-based "off-on" fluorescent reporter we recently developed, which is based on unique Fe^{2+}-mediated cleavage of N-aryl-O-acylhydroxyalamine.[29] We envisioned that the chemistry involved in the Fe^{2+} sensing of this probe could be employed to design novel Fe^{2+} responsive ABA inducers that specifically control Fe^{2+}-induced cellular effects through ABA-mediated protein dimerization (Figure 1A). Because free Fe^{2+} also exists in normal cellular environment, caged inducers of this type must be stable under normal cellular Fe^{2+} concentrations and only become activated at abnormally high Fe^{2+} concentrations. To this end, we designed and synthesized a library of ABA derivatives (**ABA-FE1** to **26**) that contain differently substituted aniline, benzyl amine and oxime derivatives conjugated to the carboxylate group of ABA through an O-N linkage (Figure 1B, Scheme S1, S2, S3). The aniline, benzylamine and oxime moieties in these substances contain a variety of electron donating and withdrawing groups to enable tuning of the reactivity of the O-N linkage against Fe^{2+}. Bulky substituents (e.g. phenyl or *t*-butyl groups) were also introduced at the benzylic position of the benzyl amine and oxime groups to adjust the lability of the ester linkage caused by cellular esterases.

To identify **ABA-FEs** that undergo Fe^{2+} specific bond cleavage and that are stable under cellular conditions (i.e. tolerating normal cellular level of Fe^{2+} and other biomolecules), we probed the reactivity and selectivity of **ABA-FEs** using a series of assays. To check their chemical stability, **ABA-FEs** were incubated in the HEPES buffer at 37°C for 1 h followed by HPLC analysis. The percentage of ABA generated from each **ABA-FE** (indicating cleavage efficiency) was quantified. In the series, **ABA-FE2** and **ABA-FE8** are not stable under these conditions (Figure S1) and therefore eliminated from further studies. To examine their relative Fe^{2+} promoted reactivity, 10 μM **ABA-FEs** were incubated with 10 and 100 eq of Fe^{2+} for 1 h followed by HPLC analysis (Figure 2A). The results show that **ABA-FE5** and **ABA-FE25** are not reactive even with the high level of Fe^{2+}. Many **ABA-FEs** displayed high reactivity in the presence of the lower level of Fe^{2+}. However, **ABA-FE16** to **21**, and **ABA-FE26** have much lower reactivity at the low Fe^{2+} concentrations but reactive at high Fe^{2+} level. Most **ABA-FEs** have low reactivity towards Fe^{3+} (Figure S2). Since **ABA-FE18** gave the most desired reactivity profile, we further tested its reactivity against various cellular molecules including metal ions (e.g. Cu^{2+}, Zn^{2+}, Mg^{2+}, Ca^{2+}, Na^{+}), oxidizing or reducing species (e.g. H_2O_2, Na_2S, cysteine, ascorbate). The results show that **ABA-FE18** is selective that undergoes cleavage reaction to give **ABA** only in the presence of high concentration of Fe^{2+} but none of the other tested molecules and ions (Figure 2B). To further characterize **ABA-FE18**, the time course of **ABA-FE18** cleavage was tested by incubating it with 100 eq of Fe^{2+} for 5 min to 24 h. The cleavage of **ABA-FE18** occurred rapidly and was near completion at 1 h (Figure S3). In addition, the dosage response of **ABA-FE18** versus different concentration of Fe^{2+} (1 to 500 eq) was also studied. It required 100 eq or higher level of Fe^{2+} to achieve significant **ABA-FE18** cleavage, although less than 50 eq also gave low to moderate level of cleavage (Figure S4).

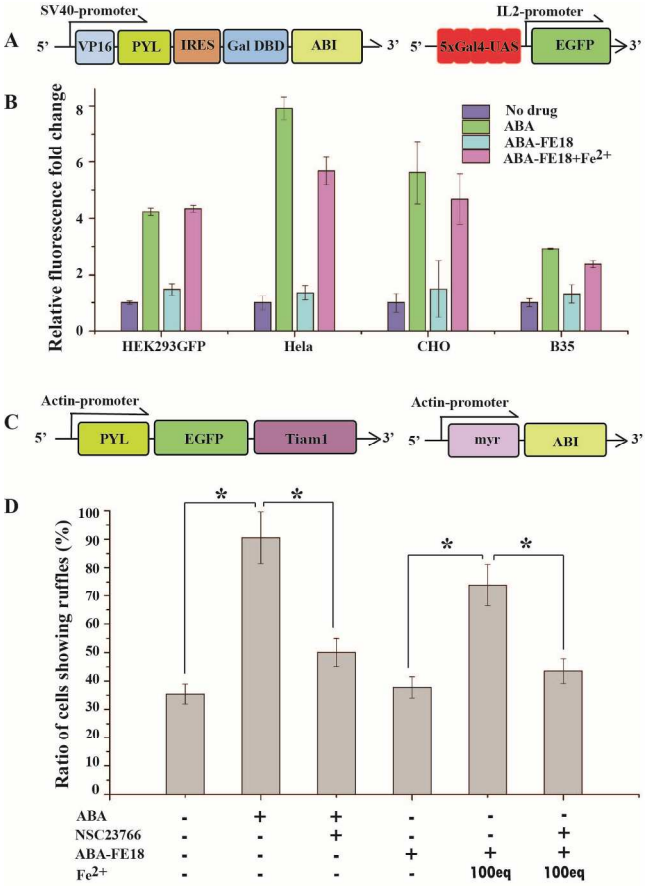

Figure 3. (A) DNA constructs for ABA-inducible EGFP expression. (B) Induced EGFP expression by ABA or Fe^{2+} in different

cells. The fold changes are calculated based on "no drug" treatment samples. (C) DNA constructs for ABA-inducible Rac1 signaling/ruffle formation. (D) Ruffle formation of CHO cells. The ratio was calculated as described in the "Methods" section. Error bars are SD (SD = 4). *P-value < 0.001.

To determine the cellular stability and reactivity of **ABA-FEs** towards Fe^{2+} in cells, a HEK293T reporter cell line was used. This cell line contains ABA-response gene cassettes stably integrated in the genome that encode a split transcriptional activator (VP-PYL/GAL4DBD-ABI) and an inducible enhanced green fluorescent protein (EGFP) with 5xUAS upstream (Figure 3A).[15] As a result, it produces EGFP in the presence of **ABA**. The cellular stability of **ABA-FE18** and other **ABA-FEs** was tested by incubating them (20 μM) with the reporter cells for 10 h. **ABA** and no drug treatment were used as positive and negative controls. The level of EGFP production, which indicates the degree of ABA-FE cleavage, was then determined using a fluorescence plate reader (Figure S5). Because the Fe^{2+} sensing units in **ABA-FEs** are linked to **ABA** through ester linkages, the endogenous cellular esterases can potentially affect the stability of **ABA-FEs** in cells. We expected that **ABA-FEs** containing bulky substituents close to the ester linkage (i.e. **ABA-FE14-26**) should have higher stability against esterases. Indeed, we observed several compounds in this group including **ABA-FE18** induced lower levels of EGFP expression (Figure S5). **ABA-EF22** to **24** induced much higher level of EGFP expression, which may be due to their higher sensitivity towards low level of Fe^{2+} (Figure 2A) or other molecules in cells.

Considering its cellular stability, Fe^{2+}-responsive characteristics and selectivity for Fe^{2+}, **ABA-FE18** was subjected to further characterization. We incubated **ABA-FE18** with EGFP reporter cells for longer time periods (up to 24 h) and observed that it is relatively stable (Figure S6), although some low levels of EGFP expression had been observed that indicates further optimization will be needed for applications requiring long incubation times. To ensure the lack of EGFP expression in the above assay was due to the superior stability of **ABA-FE18** in cells instead of the complete degradation of the compound, we also added 100 eq of Fe^{2+} in a separate experiment under the similar condition and showed that EGFP expression can be induced (Figure S6), which demonstrated that **ABA-FE18** was still functional to respond to Fe^{2+} and to generate **ABA**. We did not observe obvious cytotoxicity that can potentially be caused by the released Fe^{2+}-sensing unit. To rule out the possibility that the uncaged byproduct of **ABA-FE18** can induce observed effects, we synthesized the Fe^{2+}-sensing unit released from **ABA-FE18** after cleavage and incubated it with EGFP reporter cells. We observed no EGFP expression was induced or obvious toxicity to cells (Figure S7).

The stability of **ABA-FE18** and its ability to connect Fe^{2+} to gene activation in mammalian cells were explored. For this purpose, HEK293T EGFP reporter cells, or cells (including HeLa, B35, and CHO cells) transfected with ABA-inducible EGFP reporter plasmids (Figure 3A), were treated with 20 μM of **ABA-FE18** in the presence or absence of 100 eq of Fe^{2+} for 10 h. The induced EGFP expression was quantified in each condition using fluorescence plate reader and flow cytometer (Figure 3B, S8, S9). **ABA-FE18** was found to be reasonably stable in all tested cell lines and it readily induced EGFP expression in response to the added high level of Fe^{2+}. Based on the combined observation described above, **ABA-FE18** was identified as the optimal **ABA-FE**-based Fe^{2+}-responding inducer.

In addition to directing an external Fe^{2+} signal to induce transcriptional activation, we wanted to explore whether artificial Fe^{2+} signaling can be constructed and integrated into an endogenous signaling circuit. For this purpose, we determined if Fe^{2+} promoted release of **ABA** from **ABA-FE** can be used to induce cytoskeletal remodeling via activation of the Rac1 signaling pathway. Membrane translocation of Tiam1, a guanine exchange factor for Rac1, is sufficient to activate the Rac1 signaling pathway that leads to membrane ruffling.[30] CHO cells were transfected with DNA constructs (Figure 3C) encoding membrane-localized ABI (myr-ABI) and cytoplasmic EGFP-PYL-fused Tiam1 (PYL-EGFP-Tiam1)[15] for 24 h. The cells were then treated either with 10 μM of **ABA**, **ABA-FE18**, or **ABA-FE18** plus 100 eq of Fe^{2+} for 30 min. The membrane ruffling in all EGFP positive cells was then quantified through statistical analysis that quantified individual cell perimeters in each treated condition and compared to that from cells transfected with EGFP-PYL (see METHODS for details of analysis) using images taken by the fluorescence microscope. Obvious increases in ruffle formation were found to occur only when cells were treated with **ABA** or **ABA-FE18** plus 100 eq of Fe^{2+} (Figure 3D, S10). **ABA-FE18** alone gave a similar background level of ruffling as the condition of no-drug treatment or cells transfected only with PYL-EGFP-Tiam1 (Figure 3D, S11). To confirm that ruffle formation is induced through activation of Rac1 signaling, transfected cells were pre-treated for 1 h with 50 μM of NSC 23766, which is known to inhibit Rac1 signaling by blocking binding of Tiam1 to Rac1.[31] As expected, the presence of NSC 23766 led to a decrease in the percentage of ruffling in cells treated with **ABA** and **ABA-FE18** plus Fe^{2+} (Figure 3D).

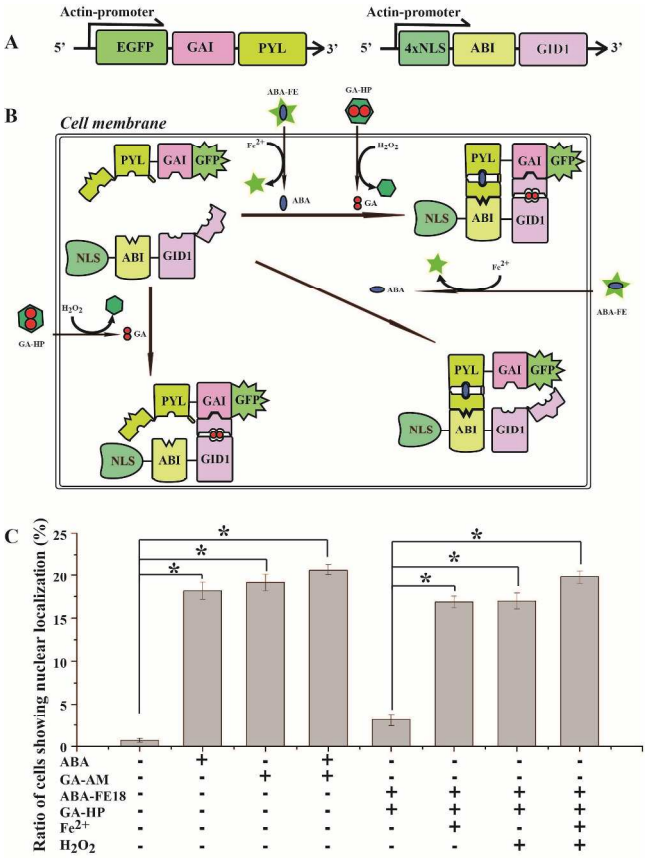

Figure 4. (A) DNA constructs of OR logic gate for EGFP nuclear translocation. (B) The design of the OR logical gate for EGFP nuclear translocation in response to stimuli. (C) Ratio of transfected CHO cells (with plasmids in (A)) showing EGFP nuclear localization after treating with different inducing signals for 1 h. Error bars are SD (N = 4). *P-value < 0.001.

To demonstrate that orthogonal signal-responsive caged CIP inducers can be incorporated to build artificial signaling networks,

ABA-FE18 and **GA-HP**[15] were used to construct two signaling networks that process different combinations of H_2O_2 and Fe^{2+} via "AND" or "OR" Boolean logic to control the nuclear translocation of EGFP. **GA-HP** is a H_2O_2-responsive caged compound containing gibberellic acid (GA),[15] which promotes the dimerization of GAI and GID1 fusion proteins.[32] To create an OR logic gate for protein translocation, DNA constructs encoding 4xNLS-ABI-GID1 and PYL-GAI-GFP fusion proteins (Figure 4A) were made. In the presence of either **ABA** or **GA**, the EGFP fusion protein should be coupled to the nuclear localization signal (NLS) and lead to nuclear localization of EGFP (Figure 4B). To validate the OR logic gate, CHO cells were transfected with both plasmids for 24 h and then treated for 30 min with 20 μM **ABA**, 100 μM **GA-AM** (acetoxymethoxy ester of **GA** to facilitate cell permeability),[32] or both **ABA** and **GA-AM**. Nuclear localization of EGFP was then quantified through statistical analysis using images taken by the fluorescence microscope (Figure 4C, S12). The results show that, as designed, either **ABA** or **GA** is sufficient to induce the EGFP translocation. To test if this logic gate system can be used to allow cells to respond to H_2O_2 and Fe^{2+}, the experiments were repeated using **ABA-FE18** and **GA-HP** in the presence or absence of 100 μM H_2O_2 and/or 100 eq Fe^{2+}. As expected, the transfected cells responded to either or both H_2O_2 and Fe^{2+} to induce the translocation of EGFP. The cleavage of **ABA-FE18** by Fe^{2+} can occur both outside and inside the cells and the generated **ABA** can freely diffuse across cell membrane to induce effects. However, the observed effects induced by H_2O_2 should be resulted from the cleavage of **GA-HP** in cells because free GA cannot pass the cell membrane.[32]

To demonstrate that a different processing algorism in response to detected signals can be engineered, we also created an AND logic gate for EGFP nuclear translocation using constructs encoding 4xNLS-GID1, GAI-ABI, and EGFP-PYL (Figure 5A, 5B). Nuclear localization of EGFP was observed to take place in transfected CHO cells only when they were treated with both **ABA** and **GA-AM** (Figure 5C). Similarly, nuclear localization of EGFP in transfected cells that are treated with **ABA-FE18** and **GA-HP** occurred only when both Fe^{2+} and H_2O_2 were present. These observations demonstrate that the cells can be reprogrammed to respond to Fe^{2+} and/or H_2O_2 and produce different biological outputs following pre-defined signal processing rules.

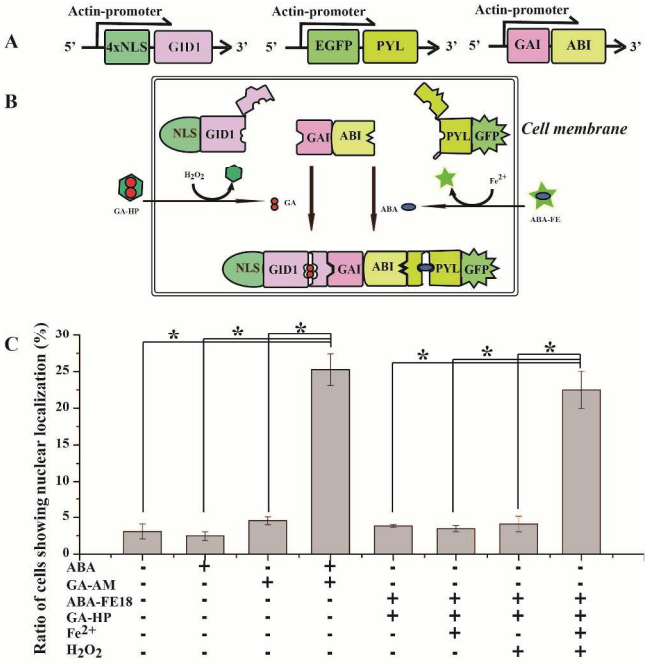

Figure 5. (A) DNA constructs of AND logic gate for EGFP nuclear translocation. (B) The design of the AND logical gate for EGFP nuclear translocation in response to stimuli. (C) Percentage of transfected CHO cells (with plasmids in (A)) showing EGFP nuclear localization after treating with different inducing signals for 1 h. Error bars are SD (N = 4). *P-value < 0.001.

In conclusion, in the investigation described above, we have developed Fe^{2+}-responsive ABA derivatives and identified **ABA-FE18** as an optimal Fe^{2+}-responsive inducer. We discovered that in general the oxime-based sensor units increased the stability of **ABA-FEs** against Fe^{2+} (e.g. **ABA-FE19 - 21** vs **22 - 24**) and electron-withdrawing substituents decreased the reactivity towards Fe^{2+} within this group (e.g. **ABA-FE17, 20, 21**). We also demonstrated that adding bulky substituents near ester linkage can increase its stability in cells. Particularly, we identified oxime as a new, stable and Fe^{2+} specific linkage (e.g., **ABA-FE18**). We believe that these observations can provide useful information for further optimization and future design of similar molecules. Our works present a unique strategy that specific sensor units can be integrated into orthogonal CIP inducers to build custom signaling pathways and logic gates responding to physiologically relevant signal cues. This new strategy should provide alternative approaches to engineer cellular signaling and responses in mammalian cells.

METHODS

Reverse-phase HPLC analysis. HPLC chromatograms were acquired using Dionex-UltiMate 3000 LC System with Acclaim 120 Å, C18, 3 μm analytical (4.6 × 100 mm) column. Chromatographic conditions: eluent A: 0.1% v/v TFA in water; eluent B: 0.1% v/v TFA in acetonitrile. **ABA** or **ABA-HP** in DMSO was eluted at a flow rate of 0.750 mL/min monitored at a wavelength of 260 nm. 0-12 min (linear): 95% A, 5% B to 5% A, 95% B; 12-15 min: 5% A, 95% B; 15-17 min (linear): 5% A, 95% B to 95% A, 5% B. Generation of **ABA** was quantified by the peak area of ABA out of the total peak area.

ABA-EFs stability test. 10 μM ABA-FE1 - 26 were incubated in 50% HEPES/DMSO (10 mM HEPES, pH7.4) for 1 h for 24 h at 37 ºC followed by HPLC assays. *Reactivity test of **ABA-FEs** towards Fe^{2+}*: 10 μM **ABA-FE1 - 26** was incubated with indicated amounts of Fe^{2+} in 50% HEPES/DMSO (10 mM HEPES, pH7.4) at 37 ºC for 1 h followed by HPLC assays. *Reactivity test of **ABA-FEs** towards Fe^{3+}*: 10 μM **ABA-FE 1 - 23** was incubated with indicated amounts of Fe^{3+} in 50% HEPES/DMSO (10 mM HEPES, pH 7.4) at 37 ºC for 1 h. HPLC results were detected right after that. *Reaction selectivity of **ABA-FE18***. 10 μM **ABA-FE18** was incubated with 100 μM (10 eq) of different molecules as indicated in 50% HEPES/DMSO (pH 7.4) at 37 ºC for 1 h and the cleavage products were detected by HPLC.

Cloning and plasmid construction. All DNA fragments were amplified by PCR from other intermediate constructs with the enzyme of Phusion DNA Polymerase (NEB) under S1000 thermal cycler with Dual 48/48 Fast Reaction Module (Bio-Rad). All the restriction enzymes used below are purchased from New England Biolabs. Actin-4xNLS-GID1 construct was derived from Actin-NES-ABI[17] by inserting 4xNLS-GID1 (gBlocks gene fragments from IDT) using SalI and NotI. Actin-GAI-ABI construct was generated from Actin-NES-ABI[17] by inserting fragment GAI-SG-linker using SalI and MluI sites. Actin-4xNLS-ABI-GID1 was generated from Actin-4xNLS-GID1 by inserting ABA using MluI site. GFP-GAI-PYL was generated from GFP-PYL[17] by inserting SG-linker-GAI-SG-linker fragment through AscI site.

Cell culture and transfection. All cells were cultured in DMEM medium (Gibco) supplemented with 10% FBS, 2 mM Gluta MAX (life technologies), 100U/mL penicillin (life technol-

ogies) and 100 μg/ml streptomycin (life technologies) at 37 ºC in a humidified atmosphere containing 5% CO_2. **EGFP expression in HEK293T EGFP cells.** HEK293T EGFP reporter cells were seeded 24 h prior to treatment in 24-well plates at 100,000/well. For stability test, cells were treated without addictive, 20 μM **ABA**, or **ABA-FE1 - 26** for 10 h (or also 18 and 24 h for ABA-FE18). Cells were then harvested and washed with PBS twice. Resulting cells were re-suspended in 100 μL of PBS and fluoresce was quantified by fluorescent plate reader. For reactivity test, cells were treated without addictive, with 20 μM **ABA**, 20 μM **ABA-FE18** only or plus 100 eq of Fe^{2+} for 10 h. Cells were then harvested, washed and quantified as above. **EGFP expression in Hela/B35/CHO cells.** Cells were seeded in 24-well plates (100,000/well for Hela and B35, 50,000/well for CHO) for 24 h. 0.3 μg SV40-VP16-PYL-ires-Gal-ABI and 0.3 μg 5xGal4-UAS-EGFP plasmids were mixed with 30 μL of Opti-MEM (life technologies) and 1.8 μL of PEI (Polysciences). After incubation at RT for 15 min, the mixture was added to the cells and cultured for 24 h. Then, cells were treated without addition, with 20 μM **ABA**, 20 μM **ABA-FE18** only or plus 100 eq of Fe^{2+} for 10 h. Then cells were harvested, washed and quantified by fluorescent plate reader as above. **Induced ruffling.** CHO were seeded over glass coverslips in 24-well plates at 50,000/well for 24 h. Then cells were transfected with 0.3 μg PYL-EGFP-Tiam1 and 0.3 μg myr-ABI DNA. After 24 h, cells were treated without addition, with 10 μM **ABA**, 10 μM **ABA-FE18** only or plus 100 eq of Fe^{2+}. For the cells treated with rac1 inhibitor NSC 23766, 50 μM NSC 23766 was added to the medium 1 h prior to drug addition. Slides were prepared 30 min after adding compounds and images were then taken using a Zeiss fluorescence microscopy for statistical analysis. **Logic gates to control EGFP translocation.** CHO were seeded over glass coverslips in 24-well plates at 50,000/well for 24 h. Cells were transfected for 24 h with 0.5 μg 4xNLS-ABI-GID1 and 0.3 μg GFP-GAI-PYL DNA for OR logic gate, or 0.3 μg 4xNLS-GID, 0.3 μg GAI-ABI and 0.2 μg GFP-PYL DNA for AND logic gate. Cells were then treated without addition, with 20 μM **ABA**, 100 μM **GA-AM**, 20 μM **ABA** & 100 μM **GA-AM**, 20 μM **ABA-FE18** & 100 μM **GA-HP**, 20 μM **ABA-FE18** & 100 μM **GA-HP** plus 2 mM Fe^{2+}, or 20 μM **ABA-FE18** & 100 μM **GA-HP** plus 100 μM H_2O_2 (**GA-AM**, **GA-HP** and H_2O_2 were added 30 min before the addition of **ABA**, **ABA-FE18** and Fe^{2+}). 30 min after adding compounds, coverslips were washed with PBS and fixed with 300 μL of 4% paraformaldehyde in PBS at room temperature for 20 min. Cells were then washed twice with PBS and incubated with 1x DAPI in the dark at the room temperature for 5 min. After a final wash with PBS, the coverslips were mounted on a glass slide with Vectashield (VWR) mounting media and images of cells were then taken using a fluorescence microscope. All cellular experiments were conducted 3 to 4 independent times and each time with triplicate or quadruplicate.

Flow cytometry analysis. Cell samples were trypsinized and washed with PBS twice. EGFP levels were analyzed by flow cytometry and 10K cells were counted for each condition. Mean fluorescence intensity for all counted cells in each condition was obtained by BD Accuri C6 Plus Flow Cytometer, which were all normalized to ABA only condition. Experiments were conducted in triplicate or quadruplicate.

Fluorescence microscopy and statistical analysis. Zeiss Axio Observer. D1 outfitted with HBO 100 microscopy illumination system (GFP: excitation 470/40 and emission 525/50) was used to take fluorescence images in the described experiments for the following statistical analysis. Cell images were collected from 5 different areas (4 quarters and center) in each of the 3 independent experiments. For each image, 100 (for membrane ruffling) to 300 (for EGFP translocation) cells were analyzed along the diagonal lines. Cells were categorized as displaying EGFP nuclear translocation when the ratio in fluorescence intensity of the cytoplasm over that of nucleus was less than one. To define ruffled cells, the range of the regular cell perimeter was first obtained by transfecting cells with the EGFP-PYL construct and then measured the perimeters of EGFP expressing cells chosen for analysis as described above using Image J. Cells were categorized as ruffled when their cell perimeter were large than the upper range of regular cell perimeters. P values were obtained by using EXCEL with the function “CHISQ.TEST”.

Chemical synthesis: All reactions were carried out in dried flasks. The reactions were monitored by TLC for completion. Commercially available reagents were used as received without further purification unless otherwise specified. Merck 60 silica gel was used for column chromatography, and Whatman silica gel plates with fluorescence F254 were used for thin-layer chromatography (TLC) analysis. ^{1}H and ^{13}C NMR spectra were recorded on Bruker Avance 300. Detailed synthesis procedures are listed in the supporting information.

ASSOCIATED CONTENT

Supporting Information

The Supporting Information is available free of charge on the ACS Publications website at DOI: xxxxxxxx

ABA-FEs synthesis (Scheme S1, S2, S3), Stability test of ABA-FEs (Figure S1), reactivity test of ABA-FEs response to Fe^{3+} (Figure S2), time course of ABA-FE18 cleavage (Figure S3), dosage response of ABA-FE18 (Figure S4), cellular stability of ABA-FEs (Figure S5 and S6), effect of uncaged byproduct of ABA-FE18 (Figure S7), flow cytometry analysis of Fe^{2+} induced EGFP expression (Figure S8, S9), representative images showing ruffled/ not ruffled cells (Figure S10), nuclear localized/ not localized cells (Figure S12), ruffle showing cells in control groups (Figure S11), primers used for PCR, synthesis procedures and characterization data for ABA-FEs.

AUTHOR INFORMATION

Corresponding Author

*fsliang@unm.edu
*wwang@unm.edu

Author Contributions

§G.Z. and H.L. contributed equally to the present work.

ACKNOWLEDGMENT

This work was supported by the Michael J. Fox Foundation for Parkinson's Research (F.-S. L., W.W., H.L.), the Jiangsu Government Scholarship for Overseas Studies (H.L.), and UNM-IMSD/NIH GM-060201-16 (L.E.B.).

REFERENCES

(1) Lienert, F., Lohmueller, J. J., Garg, A., Silver, P. A. (2014) Synthetic biology in mammalian cells: next generation research tools and therapeutics. *Nat. Rev. Mol. Cell Biol.* 15, 95-107.

(2) Bashor, C. J., Horwitz, A. A. Peisajovich, S. G., Lim, W. A. (2010) Rewiring cells: synthetic biology as a tool to interrogate the organizational principles of living systems. *Annu. Rev. Biophys.* 39, 515.

(3) Wang, Y. H., Wei, K. Y., Smolke, C. D. (2013) Synthetic biology: advancing the design of diverse genetic systems. *Annu. Rev. Chem. Biomol. Eng.* 4, 69.

(4) Aubel, D., Fussenegger, M. (2010) Mammalian synthetic biology–from tools to therapies. *BioEssays* 32, 332-345.

(5) Ruder, W. C., Lu, T., Collins, J. J. (2011) Synthetic biology moving

into the clinic. *Science (New York, N.Y.)* 333, 1248-1252.
(6) Rogers, J. K., Taylor, N. D., Church, G. M.(2016) Biosensor-based engineering of biosynthetic pathways. *Curr. Opin. Biotechnol.* 42, 84-91.
(7) Nandagopal, N., Elowitz, M. B. (2011) Synthetic biology: integrated gene circuits. *Science (New York, N.Y.)* 333, 1244-1248.
(8) Brophy, J. A., Voigt, C. A. (2011) Principles of genetic circuit design. *Nat. Methods* 11, 508-520.
(9) Miyamoto, T., Razavi, S., DeRose, R., Inoue, T. (2013) Synthesizing biomolecule-based Boolean logic gates. *ACS Synth. Biol.*2, 72-82.
(10) Slusarczyk, A. L., Lin, A., Weiss, R. (2012) Foundations for the design and implementation of synthetic genetic circuits. *Nat. Rev. Genet.* 13, 406-420.
(11) DeRose, R., Miyamoto, T., Inoue, T. (2013) Manipulating signaling at will: chemically-inducible dimerization (CID) techniques resolve problems in cell biology. *Pflugers Arch., EJP* 465, 409-417.
(12) Fegan, A., White, B., Carlson, J. C., Wagner, C. R. (2010) Chemically controlled protein assembly: techniques and applications. *Chem. Rev.* 110, 3315-3336.
(13) Gestwicki, J. E.,Marinec, P. S. (2007) Chemical control over protein-protein interactions: beyond inhibitors. *Comb. Chem. High Throughput Screen.* 10, 667-675.
(14) Chan, J., Dodani, S. C., Chang, C. J. (2012) Reaction-based small-molecule fluorescent probes for chemoselective bioimaging. *Nat. Chem.* 4, 973-984.
(15) Zeng, G., Zhang, R., Xuan, W., Wang, W., Liang, F. S. (2015) Constructing de Novo H_2O_2 Signaling via Induced Protein Proximity. *ACS Chem. Biol.* 10, 1404-1410.
(16) Wright, C. W., Guo, Z. F., Liang, F. S. (2015) Light control of cellular processes by using photocaged abscisic acid. *ChemBioChem* 16, 254-261.
(17) Liang, F. S., Ho, W. Q., Crabtree, G. R. (2011) Engineering the ABA plant stress pathway for regulation of induced proximity. *Sci. Signal.* 4, rs2.
(18) Theil, E. C., Goss, D. J. (2009) Living with iron (and oxygen): questions and answers about iron homeostasis. *Chem. Rev.* 109, 4568-4579.
(19) Breuer, W., Shvartsman, M., Cabantchik, Z. I. (2008) Intracellular labile iron. *Int. J. Biochem. Cell Biol.* 40, 350-354.
(20) Oshiro, S., Morioka, M. S., Kikuchi, M. (2011) Dysregulation of iron metabolism in Alzheimer's disease, Parkinson's disease, and amyotrophic lateral sclerosis. *Adv. Pharmacol. Sci .2011*, 378278.
(21) Jenner, P. (2003) Oxidative stress in Parkinson's disease. *Ann. Neurol.*53 Suppl 3, S26.
(22) Dixon, S. J., Stockwell, B. R. (2014) The role of iron and reactive oxygen species in cell death. *Nat. Chem. Biol.* 10, 9-17.
(23) Mercer, A. E., Maggs, J. L., Sun, X. M., Cohen, G. M., Chadwick, J., O'Neill, P. M., Park, B. K. (2007) Evidence for the involvement of carbon-centered radicals in the induction of apoptotic cell death by artemisinin compounds. *J. Biol. Chem.* 282, 9372-9382.
(24) Au-Yeung, H. Y., Chan, J., Chantarojsiri, T., Chang, C. J. (2013) Molecular imaging of labile iron (II) pools in living cells with a turn-on fluorescent probe. *J. Am. Chem. Soc.* 135, 15165-15173.
(25) Hirayama, T., Okuda, K., Nagasawa, H. (2013) A highly selective turn-on fluorescent probe for iron (II) to visualize labile iron in living cells. *Chem. Sci.* 4, 1250-1256.
(26) Li, P. L., Fang, L., Zhou, H., Zhang, W., Wang, X., Li, N., Zhong, H., Tang, B. (2011) A new ratiometric fluorescent probe for detection of Fe^{2+} with high sensitivity and its intracellular imaging applications. *Chem. Eur. J.* 17, 10520-10523.
(27) Niwa, M., Hirayama, T., Okuda, K., Nagasawa, H. (2014) A new class of high-contrast Fe (II) selective fluorescent probes based on spirocyclized scaffolds for visualization of intracellular labile iron delivered by transferrin. *Org. Biomol. Chem.* 12, 6590-6597.
(28) Spangler, B., Morgan, C. W., Fontaine, S. D., Vander Wal, M. N., Chang, C. J., Wells, J. A., Renslo, A. R. (2016) A reactivity-based probe of the intracellular labile ferrous iron pool. *Nat. Chem. Biol.* 12, 680-685.
(29) Xuan, W., Pan, R., Wei, Y., Cao, Y., Li, H., Liang, F. S., Liu, K. J., Wang, W. (2016) *Bioconjugate Chem.* 27, 302-308.
(30) Michiels, F., Habets, G. G., Stam, J. C., van der Kammen, R. A., Collard, J. G. (1995) A role for Rac in Tiaml-induced membrane ruffling and invasion. *Nature* 375, 338-340.
(31) Gao, Y., Dickerson, J. B., Guo, F., Zheng, J., Zheng, Y. (2004) Rational design and characterization of a Rac GTPase-specific small molecule inhibitor. *Proc. Natl. Acad. Sci. U.S.A.* 101, 7618-7623.
(32) Miyamoto, T., DeRose, R., Suarez, A., Ueno, T., Chen, M., Sun, T. P., Wolfgang, M. J., Mukherjee, C., Meyers, D. J., Inoue, T. (2012) Rapid and orthogonal logic gating with a gibberellin-induced dimerization system. *Nat. Chem. Biol.* 8, 465-470.

Table of Contents/Abstract Graphic

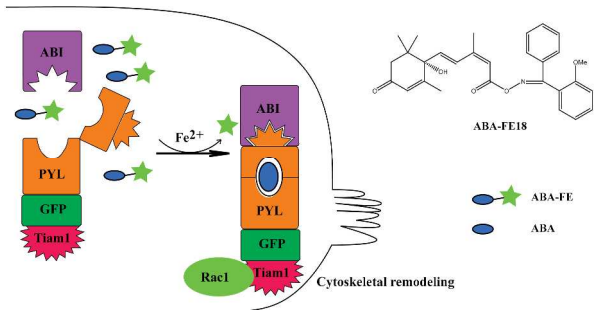

A probe, ABA-FE18, was developed that translates Fe(II) signal into tailored cellular events and used to build Fe(II)/H_2O_2 responding signal circuits.